

BeautyGRPO: Aesthetic Alignment for Face Retouching via Dynamic Path Guidance and Fine-Grained Preference Modeling

Jiachen Yang¹ Xianhui Lin^{2†} Yi Dong² Zebiao Zheng²
Xing Liu² Hong Gu² Yanmei Fang^{1,3*}

¹School of Cyber Science and Technology, Shenzhen Campus of Sun Yat-sen University, China

²vivo BlueImage Lab, vivo Mobile Communication Co., Ltd., China

³Guangdong Provincial Key Laboratory of Information Security Technology, China

[Project Page](#)

[†]Project leader *Corresponding author

Abstract

Face retouching requires removing subtle imperfections while preserving unique facial identity features, in order to enhance overall aesthetic appeal. However, existing methods suffer from a fundamental trade-off. Supervised learning on labeled data is constrained to pixel-level label mimicry, failing to capture complex subjective human aesthetic preferences. Conversely, while online reinforcement learning (RL) excels at preference alignment, its stochastic exploration paradigm conflicts with the high-fidelity demands of face retouching and often introduces noticeable noise artifacts due to accumulated stochastic drift. To address these limitations, we propose BeautyGRPO, a reinforcement learning framework that aligns face retouching with human aesthetic preferences. We construct FRPref-10K, a fine-grained preference dataset covering five key retouching dimensions, and train a specialized reward model capable of evaluating subtle perceptual differences. To reconcile exploration and fidelity, we introduce Dynamic Path Guidance (DPG). DPG stabilizes the stochastic sampling trajectory by dynamically computing an anchor-based ODE path and replanning a guided trajectory at each sampling timestep, effectively correcting stochastic drift while maintaining controlled exploration. Extensive experiments show that BeautyGRPO outperforms both specialized face retouching methods and general image editing models, achieving superior texture quality, more accurate blemish removal, and overall results that better align with human aesthetic preferences.

(a) Comparison Across Different Face Retouching Methods

Input	RetouchFormer	NanoBanana	Ours
Blemish Removal	✗	✓	✓
ID Preservation	✓ 0.9767	✗ 0.8924	✓ 0.9789
Human Preference	✗	✗	✓

(b) Different Training Paradigms

Input Setup	FluxKontext w/ LoRA		
	SFT	FlowGRPO	BeautyGRPO
	△ Suboptimal Quality	✗ Excessive Noise Artifacts	✓ High Realism & Quality

Figure 1. Comparison of face retouching methods and training paradigms. (a) Our approach outperforms specialized (RetouchFormer) and general (NanoBanana) models in blemish removal, identity preservation, and human preference. (b) By stabilizing stochastic exploration, BeautyGRPO overcomes the limitations of Supervised Fine-Tuning (SFT) and standard online RL (FlowGRPO), achieving natural and highly realistic results.

1. Introduction

With the rapid proliferation of social media and imaging devices, digital portraiture has become an integral part of daily

life, driving a growing demand for high-quality face retouching. This task is inherently complex, as it requires removing subtle imperfections such as acne and blemishes while preserving identity features such as moles, pores, and natural skin texture, in order to enhance overall aesthetic appeal. In essence, face retouching must strike a balance between high visual fidelity to the original portrait and consistency with subjective human aesthetic preferences.

To address this challenge, researchers have explored a variety of specialized architectures, ranging from CNN-based [20, 37] to advanced Transformer-based models [44–46, 54, 55]. Recently, general image editing models [11, 24, 30, 35, 59] have also shown strong potential for face retouching. However, most existing methods still depend on supervised learning, either training from scratch or supervised fine-tuning (SFT). The limitation of such supervised objectives lies not only in the scarcity of curated data, but also in their pixel-level learning targets. They train models to imitate labeled reference images rather than to align with human aesthetic preferences. This objective enforces local fidelity while neglecting perceptual alignment, leading to results that may be faithful to the labels but still misaligned with human aesthetic expectations. As a result, the outputs often exhibit visually rigid or unnatural retouching effects, as illustrated in Fig. 1. Moreover, by constraining optimization to pixel-level reconstruction, supervised learning encourages overfitting to specific retouching styles and prevents the model from discovering solutions that surpass the aesthetic quality of the training data. This observation raises a fundamental question: **Can we align face retouching with human preferences?**

Reinforcement learning (RL) has recently emerged as a promising framework for aligning image generation with human preferences [4, 7, 10, 13, 32–34, 40, 41, 56, 58, 60]. In text-to-image (T2I) generation, methods such as FlowGRPO [22] demonstrate strong controllability by integrating online RL into flow-matching models [9, 18, 21, 25]. This online RL mechanism enables active exploration, allowing the model to discover solutions beyond those observed during supervised training and to better align with human judgment. Despite these successes, directly applying T2I-RL frameworks to face retouching introduces two fundamental challenges. The first is the conflict between fidelity and exploration. To encourage exploration, FlowGRPO injects stochastic noise into the sampling process, converting the deterministic ODE trajectory into a stochastic differential equation (SDE). While this stochasticity enhances diversity in T2I generation, it is detrimental to face retouching, where visual stability and precision are essential. As shown in Fig. 1, the accumulated noise causes the trajectory to deviate from the high-fidelity manifold and produce noticeable noise artifacts. The second challenge lies in the granularity of reward supervision. Existing reward models for T2I

generation or general image editing [26, 43, 48, 49, 51, 52] mainly focus on global aesthetics or instruction following. They lack the fine-grained perceptual sensitivity required for face retouching, which depends on accurate evaluation of skin smoothing, blemish removal, texture preservation, and identity consistency.

In this paper, we propose BeautyGRPO, a RL framework that aligns face retouching with human aesthetic preferences. A key challenge in this domain is the lack of reward models capable of assessing fine-grained retouching quality. To address this, we construct FRPref-10K, a large-scale **face retouching preference** dataset covering five key dimensions: skin smoothing, blemish removal, texture quality, clarity, and identity preservation. Each image is evaluated by multiple vision-language models (VLMs) through reasoning-based scoring, followed by human refinement to ensure alignment with aesthetic judgment. Based on this dataset, we train a reward model that captures subtle perceptual differences between retouched image pairs and reflects human preferences.

To resolve the critical conflict between fidelity and exploration, we introduce Dynamic Path Guidance (DPG), the core algorithm of BeautyGRPO. DPG stabilizes the stochastic trajectory by softly guiding it toward an ideal deterministic path while retaining controlled stochasticity. Unlike SFT, which explicitly aligns model outputs with label images through pixel-level supervision, DPG incorporates label images only within the sampling process as stability anchors. These anchors are high-preference exemplars selected from our FRPref-10K dataset and serve to regularize the trajectory around a high-fidelity manifold rather than act as paired ground-truth references. The anchors provide gentle directional stabilization, keeping the sampling trajectory close to a high-fidelity manifold without interfering with the reward-driven optimization. This design allows the policy to move beyond the anchor when higher rewards suggest more appealing results, preserving the exploratory nature of online RL while maintaining trajectory stability. Through this anchored yet reward-driven mechanism, DPG establishes a balanced regime between exploration and fidelity, effectively preventing trajectory drift while enabling the discovery of retouching results that surpass the aesthetic quality of the reference data.

Our contributions are summarized as follows:

1. We construct FRPref-10K, a large-scale and fine-grained face retouching preference dataset, and train a specialized reward model that captures multi-dimensional human aesthetic preferences with high accuracy.
2. We propose BeautyGRPO, a reinforcement learning framework equipped with Dynamic Path Guidance, which effectively balances exploration and fidelity during the retouching process.
3. Extensive experiments demonstrate that the proposed reward model aligns closely with human aesthetic judg-

ments, and BeautyGRPO achieves superior user preference over existing methods, particularly in skin smoothing, blemish removal, and texture preservation.

2. Related Work

2.1. Face Retouching

Face retouching aims to remove facial imperfections and enhance facial aesthetics while preserving facial identity features. Early works progress from traditional filtering [1, 3, 39] and restoration methods [23, 44, 45] to CNN-based models [20, 50, 53] and more recently to Transformer-based architectures [46, 54, 55]. Most of these specialized retouching models still rely on supervised learning. The limitation lies in their objective to align outputs with label images at the pixel level rather than with human aesthetic preferences. Furthermore, large-scale general image editing models [11, 24, 30, 47, 59] can perform complex retouching operations through instruction-driven editing, but they often introduce visually unnatural effects such as altered facial identity, oily or plastic-like skin texture, and false visual artifacts, leading to inconsistent and less realistic results.

2.2. Reinforcement Learning for Diffusion Models

Reinforcement learning has emerged as an effective approach for aligning diffusion and flow-matching models with human preferences. Policy-gradient methods such as DDPO [4] and DPOK [10] optimize preference scores, but the long gradient paths in diffusion models limit updates to only a few late timesteps. DiffusionDPO [40] extends DPO [34] to T2I generation in an offline setting using paired positive and negative samples. This yields stable optimization but remains constrained by the quality and diversity of static data and has limited capacity to go beyond the training distribution. Online RL methods such as FlowGRPO [22] adapt GRPO [12] to flow-matching models by converting the deterministic ODE into an SDE to enable active exploration. When applied to face retouching, SDE-based exploration introduces random drift that violates high-fidelity constraints and leads to residual artifacts. While such stochasticity is valuable for diversity in text-to-image generation, it conflicts with the precision and stability required for portrait enhancement.

2.3. Reward Modeling for Human Preferences

Reward models are central to reinforcement learning, serving as the optimization signal that aligns model behavior with human preferences. Recent advances in T2I generation and image editing achieve such alignment by training reward models on large-scale human preference datasets [17, 49]. Representative models include ImageReward [51], HPSv2 [49], and UnifiedReward [43] for T2I generation, and EditScore [26], EditReward [48], and UnifiedReward-Edit [43] for image editing. While these reward models

align generation with human aesthetic judgments, they focus mainly on global image quality and text-image consistency. They fail to capture subtle perceptual dimensions such as the balance between skin smoothness and texture naturalness, and the cleanliness of blemish removal. To bridge this gap, we construct a dedicated face retouching preference dataset and train a reward model that provides fine-grained reward guidance aligned with human aesthetic preferences.

3. Methodology

We introduce BeautyGRPO, a reinforcement learning framework that aligns face retouching models with human aesthetic preferences. It consists of three components: (1) a large-scale, multi-dimensional preference dataset (Section 3.1); (2) a specialized reward model for fine-grained aesthetic evaluation (Section 3.2); and (3) the Dynamic Path Guidance (DPG) algorithm, which stabilizes online RL by reconciling stochastic exploration with deterministic fidelity (Section 3.3).

3.1. Fine-Grained Preference Data Curation

Aesthetic alignment requires data that reflect the nuanced judgments inherent in face retouching. To overcome the limitations of existing coarse datasets, we construct FRPref-10K, a fine-grained dataset of 10,000 high-resolution preference pairs with detailed multi-dimensional annotations.

Data Collection and Candidate Generation. We curated source portraits from the FFHQR [36] and a proprietary high-resolution collection, ensuring diverse demographics and imaging conditions. For each input image I_{in} , we generate a diverse pool of retouched candidates $\{I_{out}^i\}$ using multiple state-of-the-art models (NanoBanana [11], Flux.1 Kon-text [19], RetouchFormer [46]) with varied random seeds. Preference pairs (I_{in}, I_A, I_B) are then constructed through both inter-model comparison (output vs. output) and output-vs-label evaluation. More details regarding the dataset statistics are provided in the supplementary material E.

Hybrid VLM-Human Annotation Pipeline. We employ a three-stage annotation protocol that combines the reasoning ability of large VLMs with human verification:

1. **Multi-Dimensional Assessment:** We define five critical aesthetic dimensions: Skin Smoothing, Blemish Removal, Texture Quality, Clarity, and Identity Preservation. An ensemble of VLMs (GPT-4o [31], Qwen2.5-VL-72B [2], Gemini 2.5 Pro [8]) evaluates each pair across these dimensions, providing both quantitative scores and structured reasoning. VLM outputs are aggregated to form an initial consensus. Trained human annotators subsequently audit these assessments under identical criteria.
2. **Expert Adjudication:** Discrepancies between human judgment and the VLM consensus are escalated to senior experts for final arbitration.

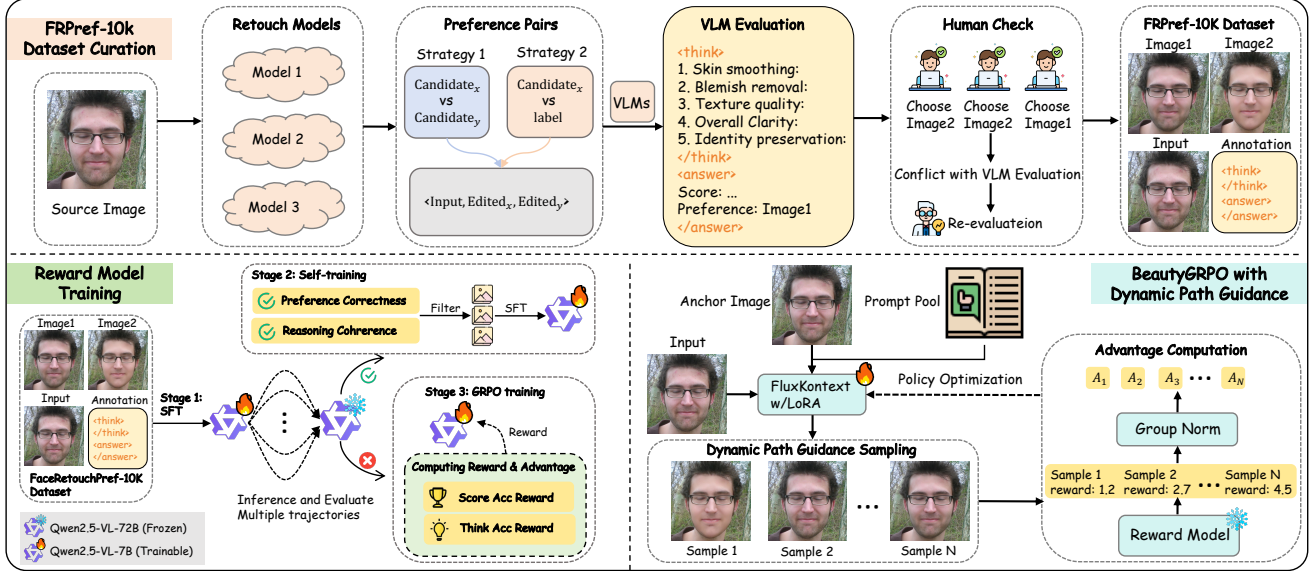


Figure 2. Overview of our FRPref-10K construction, reward model training, and BeautyGRPO with Dynamic Path Guidance (DPG). **Top:** FRPref-10K dataset curation pipeline. Multiple retouched candidates are generated with diverse editing models, preference pairs are formed via output-vs-output/label comparisons, and are annotated by VLMs across five quality dimensions before human verification. **Bottom left:** Three-stage reward model training, including SFT, self-training with consistency filtering, and GRPO. **Bottom right:** BeautyGRPO training with DPG on a FluxKontext-LoRA backbone.

3.2. Multi-Dimensional Retouching Reward Model

Leveraging FRPref-10K, we train a specialized reward model $R_\phi(I_{in}, I_{out})$ capable of providing dense, interpretable feedback. Following the UnifiedReward-Thinking paradigm [42], we adopt a three-stage training strategy to enhance reasoning quality, initializing from Qwen2.5-VL-7B [2].

Stage 1: Structured Reasoning Initialization We perform SFT on a 2K subset to adapt the model to generate structured reasoning across five dimensions in a <think> block and a final preference decision in an <answer> block.

Stage 2: Self-Training with Consistency Filtering The Stage 1 model generates multiple reasoning trajectories for the remaining 8K samples. We employ a consistency filtering mechanism based on two criteria: *Preference Correctness* (alignment with ground truth) and *Reasoning Coherence* (semantic consistency between reasoning and decision, evaluated by a high-capacity VLM). Consistent trajectories are utilized for a subsequent round of SFT, reinforcing reliable reasoning patterns.

Stage 3: Robustness Enhancement via GRPO For inconsistent samples, we apply GRPO [12] to improve robustness. The model explores diverse reasoning paths, evaluated by both outcome rewards (preference accuracy) and process rewards (reasoning coherence, assessed by a lightweight verifier such as DeBERTa-V3 [14]). This reinforcement phase strengthens the model’s ability to produce stable and human-aligned aesthetic judgments.

3.3. BeautyGRPO with Dynamic Path Guidance

We use the trained reward model as feedback to align a flow-matching image editing policy model π_θ . We extend the FlowGRPO framework [22] with a novel Dynamic Path Guidance (DPG) mechanism that stabilizes SDE-based exploration for high-fidelity retouching tasks.

3.3.1. Preliminaries: The Fidelity-Exploration Conflict

Flow-matching models [21, 25] learn a vector field $v_\theta(x_t, t)$ that transports a noise distribution $p_1(x)$ toward a data distribution $p_0(x)$ through a deterministic ODE trajectory. To enable exploration for online RL, FlowGRPO [22] converts this ODE into a SDE formulation by injecting noise:

$$dx_t = \left[v_\theta(x_t, t) + \frac{\sigma_t^2}{2t} (x_t + (1-t)v_\theta(x_t, t)) \right] dt + \sigma_t d\omega, \quad (1)$$

where $d\omega$ represents standard Brownian motion, and $\sigma_t = \eta \sqrt{\frac{t}{1-t}}$ controls the noise level. This stochastic term induces diverse sampling trajectories, allowing the policy to receive richer, more differentiated reward signals. Specifically, given G generated samples $\{x_0^i\}_{i=1}^G$ with corresponding rewards $R(x_0^i)$, FlowGRPO normalizes these rewards into standardized advantages:

$$\hat{A}^i = \frac{R(x_0^i) - \text{mean}(\{R(x_0^i)\}_{i=1}^G)}{\text{std}(\{R(x_0^i)\}_{i=1}^G)}. \quad (2)$$

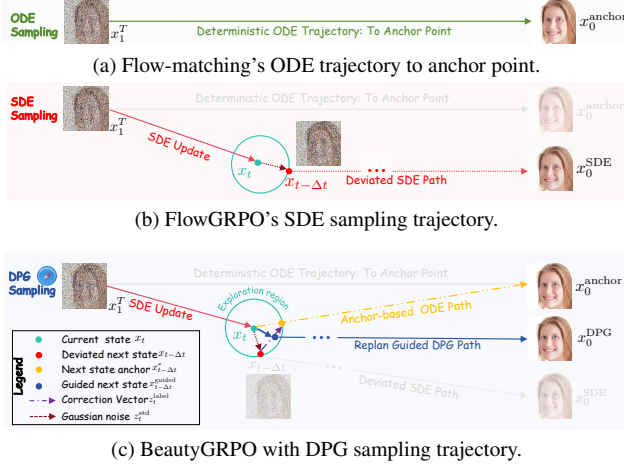


Figure 3. Overview of different sampling trajectories. (a) Standard flow-matching ODE trajectory for SFT. (b) Uncontrolled SDE trajectory in FlowGRPO, which gradually drifts from the high-fidelity anchor point and introduces noise artifacts. (c) Proposed BeautyGRPO with Dynamic Path Guidance (DPG). At each timestep, DPG dynamically computes an anchor-based ODE path and replans a guided trajectory by linearly blending a correction vector with standard Gaussian noise, correcting stochastic drift while maintaining controlled exploration.

The policy is optimized by the GRPO objective:

$$\mathcal{L}(\theta) = \mathbb{E}_{c \sim \mathcal{C}, \{x^i\}_{i=1}^G \sim \pi_{\theta_{\text{old}}}} \left[\frac{1}{G} \sum_{i=1}^G \frac{1}{T} \sum_{t=0}^{T-1} \min \left(r_t^i(\theta) \hat{A}_t^i, \text{clip} \left(r_t^i(\theta), 1 - \varepsilon, 1 + \varepsilon \right) \hat{A}_t^i \right) \right], \quad (3)$$

where $r_t^i(\theta) = \frac{p_{\theta}(x_{t-1}^i | x_t^i)}{p_{\theta_{\text{old}}}(x_{t-1}^i | x_t^i)}$ denotes the per-step likelihood ratio between old policy model $\pi_{\theta_{\text{old}}}$ and updated model π_{θ} .

While the stochastic term $\sigma_t \sqrt{dt} \epsilon$ in Eq. 1 enhances exploration in general T2I generation, it conflicts with the high-fidelity demands of face retouching. The sampling trajectory is gradually pushed away from the high-fidelity manifold by the accumulated noise, leading to uncontrolled drift and noticeable visual artifacts.

3.3.2. Dynamic Path Guidance (DPG) for Anchored Exploration

To reconcile the conflict between exploration and fidelity, we propose Dynamic Path Guidance (DPG). DPG performs anchored exploration by stabilizing the SDE trajectory near a high-fidelity manifold while still allowing deviations guided by the reward signal.

The Stability Anchor. We use high-preference samples from our FRPref-10K dataset as stability anchors, denoted

by x_0^{anchor} . The anchor is introduced only in the sampling process and is not treated as a supervision target as in SFT. Its role is to constrain the stochastic trajectory to a high-fidelity manifold, within which the policy can still explore and optimize for higher-reward retouching results.

SDE Formulation and Drift. The FlowGRPO SDE update (Eq. 1) can be expressed compactly as:

$$x_{t-\Delta t} = \mu_t + \sigma_{\text{step}} z_t, \quad z_t \sim \mathcal{N}(0, I), \quad (4)$$

where μ_t is the drift term predicted by the model:

$$\mu_t = x_t + \left[v_{\theta}(x_t, t) + \frac{\sigma_t^2}{2t} (x_t + (1-t)v_{\theta}(x_t, t)) \right] \Delta t, \quad (5)$$

and $\sigma_{\text{step}} = \sigma_t \sqrt{\Delta t}$ is the step-wise standard deviation. As illustrated in Fig. 3b, repeated application of this update gradually accumulates stochastic drift that drives the trajectory away from the high-fidelity manifold.

Dynamic Trajectory Replanning. To counteract drift accumulation, DPG dynamically replans a guided trajectory toward the anchor at each timestep. As illustrated in Fig. 3c, given the current state x_t , we replan a straight line ODE trajectory connecting x_t to the anchor x_0^{anchor} . The corresponding target state at the next timestep $s = t - \Delta t$ on this anchor-guided path is:

$$x_{t-\Delta t}^* = \left(\frac{\Delta t}{t} \right) x_0^{\text{anchor}} + \left(1 - \frac{\Delta t}{t} \right) x_t. \quad (6)$$

Guided Correction with Controlled Stochasticity. We guide the SDE update toward $x_{t-\Delta t}^*$ by introducing a correction vector z_t^{anchor} that aligns the predicted mean μ_t with this anchor-guided target:

$$z_t^{\text{anchor}} = \frac{x_{t-\Delta t}^* - \mu_t}{\sigma_{\text{step}}}. \quad (7)$$

This vector indicates the direction that steers the trajectory back toward the anchor-guided path.

However, strictly following z_t^{anchor} would collapse exploration into deterministic imitation, preventing the RL from surpassing the anchor's quality. To prevent this, we construct a blended noise vector z_t^{mix} by linearly combining the correction vector with standard Gaussian noise $z_t^{\text{std}} \sim \mathcal{N}(0, I)$:

$$z_t^{\text{mix}} = \lambda(t) z_t^{\text{anchor}} + (1 - \lambda(t)) z_t^{\text{std}}, \quad (8)$$

where $\lambda(t) = \frac{t}{\max(1, T-1)}$ is a time-dependent coefficient that decreases along the reverse-time trajectory. Thus, early reverse timesteps use stronger anchor guidance to correct structural deviations, while later timesteps rely more on stochastic noise to encourage fine-grained exploration.

Substituting z_t^{mix} into the SDE update rule in Eq. 4 yields the DPG formulation:

$$\begin{aligned} x_{t-\Delta t}^{\text{guided}} &= \mu_t + \lambda \sigma_{\text{step}} z_t^{\text{anchor}} + (1 - \lambda) \sigma_{\text{step}} z_t^{\text{std}} \\ &= (1 - \lambda) \mu_t + \lambda x_{t-\Delta t}^* + (1 - \lambda) \sigma_{\text{step}} z_t^{\text{std}}. \end{aligned} \quad (9)$$

Table 1. Quantitative evaluation of state-of-the-art methods on the FFHQR and In-the-wild datasets, utilizing diverse no-reference metrics to assess perceptual quality and aesthetic appeal. Our BeautyGRPO significantly outperforms specialized retouching models, general editing baselines, and alternative RL strategies across nearly all benchmarks. These results validate the effectiveness of our preference alignment framework in achieving high-quality, natural retouching outcomes that generalize well across diverse scenarios. Best results are in **bold**.

	FFHQR								In-the-wild						
	NIQE↓	NIMA↑	MUSIQ↑	MANIQA↑	NRQM↑	TOPIQ↑	FID↓	ArcFace↑	NIQE↓	NIMA↑	MUSIQ↑	MANIQA↑	NRQM↑	TOPIQ↑	ArcFace↑
	<i>Retouch Model</i>														
ABPN[20]	11.152	4.861	4.599	1.027	8.219	0.611	4.713	0.971	11.979	5.005	4.651	0.997	7.019	0.603	0.968
RestoreFormer[44]	12.281	4.712	4.361	0.958	7.411	0.587	15.898	0.799	12.801	4.819	4.534	0.978	7.372	0.601	0.761
RestoreFormer++[45]	12.144	4.618	4.273	0.935	7.415	0.572	15.311	0.907	12.624	4.713	4.386	0.959	7.307	0.594	0.890
VRetouchEr[54]	12.948	4.586	4.169	0.962	6.167	0.551	2.229	0.978	13.605	4.658	4.308	0.957	5.635	0.565	0.974
RetouchFormer[46]	11.153	4.723	4.465	1.036	8.175	0.605	2.275	0.986	12.996	4.712	4.501	0.999	6.753	0.593	0.976
	<i>General Editing Model</i>														
ICEdit [59]	12.502	4.645	4.192	0.978	7.424	0.555	2.818	0.967	13.016	4.175	4.371	0.967	6.610	0.567	0.949
SeedDream4.0[35]	15.033	4.804	4.503	0.993	7.538	0.571	12.314	0.893	16.812	4.979	4.638	0.966	6.371	0.573	0.898
NanoBanana[11]	11.301	4.919	4.681	1.009	8.065	0.621	6.804	0.889	12.043	5.131	4.783	0.989	6.935	0.632	0.881
Flux.K w/LoRA[19]	12.913	4.694	4.459	1.035	8.009	0.601	1.735	0.973	12.501	4.751	4.524	0.978	6.468	0.586	0.968
	<i>Reinforcement Learning Model</i>														
Flux.K+LoRA w/FlowGRPO[22]	15.024	4.573	4.271	0.935	7.132	0.571	15.657	0.882	13.513	4.687	4.391	0.958	5.844	0.572	0.879
Flux.K+LoRA w/Ours	10.831	5.123	4.906	1.079	8.401	0.676	4.054	0.952	11.821	5.357	4.982	1.052	7.526	0.674	0.944

which stabilizes online exploration and enables the policy to discover retouching results that achieve higher rewards and better aesthetics than the anchor itself.

Log Probability for Policy Optimization. For the GRPO optimization (Eq. 3), we require the transition probability $p_\theta(x_{t-\Delta t} | x_t)$ under the guided update rule. From Eq. 9, this conditional distribution follows a Gaussian $\mathcal{N}(\mu_{\text{new}}, \sigma_{\text{new}}^2 I)$ where $\mu_{\text{new}} = (1 - \lambda)\mu_t + \lambda x_{t-\Delta t}^*$ and $\sigma_{\text{new}} = (1 - \lambda)\sigma_{\text{step}}$. The corresponding log-likelihood is given by:

$$\log p_\theta(x_{t-\Delta t} | x_t) = -\frac{\|x_{t-\Delta t} - \mu_{\text{new}}\|_2^2}{2\sigma_{\text{new}}^2} - C, \quad (10)$$

where C denotes constant normalization terms. These per-step probabilities are used to compute the likelihood ratio $r_t(\theta)$ for policy updates. To reduce computation, we divide the full sampling trajectory into $K = 3$ segments, apply DPG update to one randomly selected timestep in each segment, and perform ODE updates for the others.

4. Experiments

This section validates BeautyGRPO through quantitative, qualitative, and user study comparisons against state-of-the-art methods, followed by ablation studies on our reward model and the Dynamic Path Guidance (DPG) mechanism. Further experimental details, settings, and results are provided in the supplementary material due to page limitations.

4.1. Experiments Setup

Training setup. For all open-source baselines, we perform LoRA [15] using editing triplets (prompt, input, edited) constructed from our FRPref-10K dataset. For our main study, we adopt FluxKontext [19] as the backbone and apply the same LoRA fine-tuning on these triplets. Starting from this LoRA-adapted backbone, we conduct RL with FlowGRPO and BeautyGRPO respectively, using the same set of triplets

for both. In each case, the GRPO objective in Eq. 3 is optimized with rewards predicted by our retouching reward model. The test set contains 1,000 portraits from FFHQR and 1,000 in-the-wild images collected from the Internet. All experiments are run on 8 H20 GPUs.

Evaluation metrics. Face retouching is inherently subjective, so we adopt no-reference perceptual and aesthetic metrics that approximate human judgment. We use NIQE [29] and NRQM [27] to assess overall naturalness, NIMA (AVA) [38], MUSIQ (AVA) [16], MANIQA [57], and TOPIQ (GFIQA) [6] to measure aesthetic quality, and ArcFace scores to evaluate facial quality and identity preservation. In addition, we report FID on FFHQR to quantify distributional realism. Detailed rationales for metric selection and evaluation specifics are provided in the supplementary material D.1.

4.2. Main Results

4.2.1. Quantitative results

Table 1 reports the quantitative comparison on FFHQR and the in-the-wild test set. For face retouching, the quality of a result is ultimately judged by human aesthetic perception when comparing the input and the retouched image, rather than by pixel-level match with a limited set of reference labels. Full-reference metrics such as PSNR, SSIM, and LPIPS mainly measure pixel fidelity to these references and therefore do not reliably reflect perceived naturalness or visual appeal. We thus focus on no-reference perceptual and aesthetic metrics that better capture naturalness, realism, and aesthetic quality. As shown in Table 1, BeautyGRPO outperforms all baselines on both datasets. On FFHQR, it achieves the best scores on all six no-reference metrics, with clear gains in NIMA, MUSIQ, MANIQA, NRQM, and TOPIQ and a noticeably lower NIQE. Furthermore, we evaluate our method on an in-the-wild dataset of 1000 internet portrait images. Similar improvements on this set indicate that these

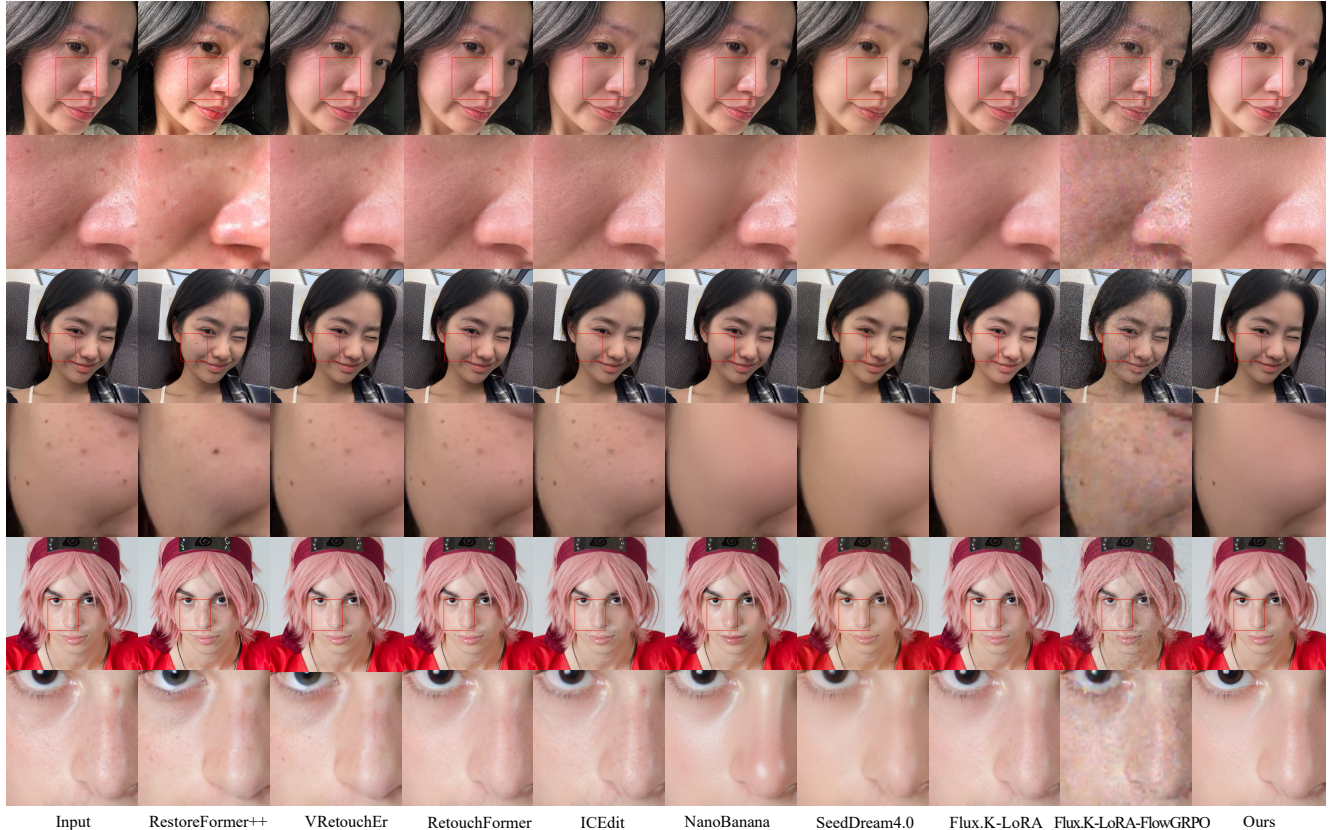


Figure 4. Visual comparison of face retouching results across different methods on FFHQR and in-the-wild datasets, where Flux.K denotes FluxKontext. Our BeautyGRPO removes blemishes cleanly while retaining natural texture, skin gloss, and moles, unlike existing models that exhibit incomplete blemish removal, over-smoothing, or artificial appearance. Please refer to the supplementary materials for more results.

benefits generalize beyond the curated dataset. Although the FID of BeautyGRPO is slightly higher than that of the best supervised baseline, this is expected. By explicitly optimizing for human preference, BeautyGRPO explores a broader range of plausible retouching styles and moves beyond the dataset-specific label distribution that FID relies on, discovering solutions that better align with human aesthetic judgments than those represented in the training labels. While aesthetic enhancements inherently require texture and structure adjustments that slightly impact identity similarity, our method maintains high ArcFace scores (0.952 on FFHQR, 0.944 in-the-wild) to ensure robust identity preservation.

4.2.2. Visualization results

Fig. 4 shows visual comparisons of face retouching results across different methods. Specialized retouching models like RetouchFormer and VRetouchEr often exhibit inaccurate blemish detection, incomplete blemish removal, and excessive smoothing that erases skin texture. General editing models like NanoBanana and SeedDream4.0 tend to overedit the face, misidentifying moles as defects and pro-

Table 2. Comparison of user preference win rates for various face retouching methods.

	VretouchEr	RetouchFormer	NanoBanana	Kontext Lora	Ours
Win rate	6.50	8.50	9.75	12.00	63.25

ducing an unnaturally glossy, synthetic appearance. In contrast, our BeautyGRPO removes facial blemishes cleanly while preserving skin texture, pores, natural gloss, and balanced skin tone, and retaining distinctive features such as moles, yielding a natural and visually refined result with excellent identity consistency.

4.3. User Study

We conduct a user study with 100 participants of different ages and editing skill levels on 20 randomly selected test cases. The study contains two questionnaires. In Questionnaire I, each question shows one original portrait and five retouched results from different methods, and participants choose the image they prefer most. In Questionnaire II, each

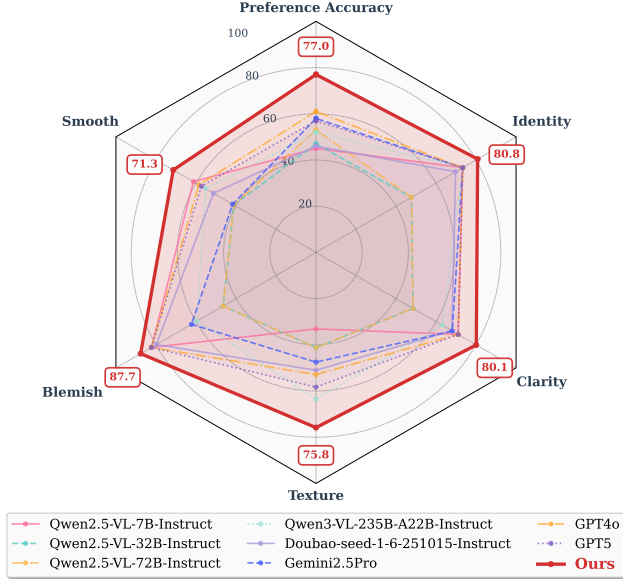


Figure 5. Radar chart comparing human judgment accuracy for our reward model against various VLMs.

question shows one original image and one retouched result, and participants rate the retouching on five perceptual dimensions, namely skin smoothing, blemish removal, texture quality, clarity, and identity preservation, using a 5-point scale. As shown in Table 2, our method achieves clearly higher win rates, indicating stronger alignment with human aesthetic preferences. Fig. 5 compares our reward model with other VLMs in terms of scoring accuracy on the five dimensions and the final preference score, showing that our reward model captures fine-grained retouching preferences more reliably. Further details of the user study setup are provided in the supplementary materials.

4.4. Ablation study

4.4.1. Reward Model

We integrate BeautyGRPO with various edit reward models on FluxKontext-LoRA, as reported in Table 3. Existing reward models mainly assess coarse image-instruction alignment and global perceptual quality, making them suboptimal for face retouching. In contrast, our reward model provides fine-grained reward modeling on five key dimensions, leading to consistent gains across all metrics.

4.4.2. BeautyGRPO on Qwen-Image-Edit

We further evaluate backbone generalization by applying BeautyGRPO to Qwen-Image-Edit [47]. As shown in Table 4, our BeautyGRPO-trained variant outperforms both the official pretrained and LoRA-tuned models on all metrics. As shown in Fig. 6, the pretrained model produces unrealistic faces with identity shifts, and the LoRA-tuned model



Figure 6. Face retouching results of Qwen-Image-Edit with various training paradigms.

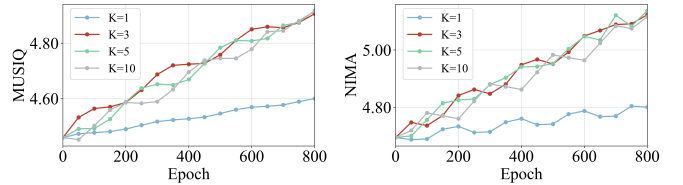


Figure 7. Ablation of DPG steps K on FFHQR.

Table 3. Quantitative evaluation of BeautyGRPO across various reward models on FFHQR.

	NIMA \uparrow	MUSIQ \uparrow	MANIQA \uparrow	TOPIQ \uparrow
EditReward[48]	4.754	4.462	1.028	0.613
EditScore[26]	4.737	4.576	1.045	0.621
UnifiedReward-Edit[43]	4.756	4.571	1.037	0.625
Our Reward Model	5.123	4.906	1.079	0.676

Table 4. Quantitative comparison of Qwen-Image-Edit variants, demonstrating the superior performance of integrating BeautyGRPO.

	NIMA \uparrow	MUSIQ \uparrow	MANIQA \uparrow	TOPIQ \uparrow
Qwen-Image-Edit	4.571	4.535	0.991	0.563
Qwen-Image-Edit+LoRA	4.824	4.745	1.028	0.595
Qwen-Image-Edit+LoRA w/Ours	5.351	5.133	1.075	0.664

still leaves blemishes and over-smooths skin, whereas BeautyGRPO achieves cleaner blemish removal and more natural skin texture, thereby yielding more realistic and visually pleasing results.

4.4.3. Different Guided SDE Step K

We conduct an ablation study on the number of Dynamic Path Guidance (DPG) steps K used during sampling. As shown in Fig. 7, the MUSIQ and NIMA scores at $K = 3$ are comparable to those at $K = 5$, while requiring fewer DPG updates and thus enabling faster sampling. Therefore, we adopt $K = 3$ as the default setting.

5. Conclusion

We present BeautyGRPO, an RL-based approach designed to align face retouching with human aesthetic preferences under high-fidelity constraints. We construct the FRPref-10K dataset and train a reward model that performs fine-grained reward modeling of face retouching quality. In addition, we introduce DPG to reconcile stochastic exploration with stable, high-fidelity sampling trajectories. Extensive experiments and user studies demonstrate that BeautyGRPO produces high-quality retouching results that are more consistent with human aesthetic preferences.

Acknowledgments

The authors would like to thank the support of Guangdong Provincial Key Laboratory of Information Security Technology (Grant No.2023B1212060026), Guangdong Provincial Key Laboratory of Intelligent Information Processing and Shenzhen Key Laboratory of Media Security (Grant No.2023B1212060076). This work was completed during the first author’s internship at vivo BlueImage Lab, vivo Mobile Communication Co.,Ltd., China.

References

- [1] Kaoru Arakawa. Nonlinear digital filters for beautifying facial images in multimedia systems. In *2004 IEEE International Symposium on Circuits and Systems (IEEE Cat. No. 04CH37512)*, pages V–V. IEEE, 2004. 3
- [2] Shuai Bai, Keqin Chen, Xuejing Liu, Jialin Wang, Wenbin Ge, Sibao Song, Kai Dang, Peng Wang, Shijie Wang, Jun Tang, et al. Qwen2. 5-vl technical report. *arXiv preprint arXiv:2502.13923*, 2025. 3, 4, 5
- [3] Nazre Batoool and Rama Chellappa. Detection and inpainting of facial wrinkles using texture orientation fields and markov random field modeling. *IEEE transactions on image processing*, 23(9):3773–3788, 2014. 3
- [4] Kevin Black, Michael Janner, Yilun Du, Ilya Kostrikov, and Sergey Levine. Training diffusion models with reinforcement learning. In *Proceedings of the International Conference on Learning Representations*, 2024. 2, 3
- [5] Yochai Blau and Tomer Michaeli. The perception-distortion tradeoff. In *Proceedings of the IEEE conference on Computer Vision and Pattern Recognition*, pages 6228–6237, 2018. 4
- [6] Chaofeng Chen, Jiadi Mo, Jingwen Hou, Haoning Wu, Liang Liao, Wenxiu Sun, Qiong Yan, and Weisi Lin. Topiq: A top-down approach from semantics to distortions for image quality assessment. *IEEE Transactions on Image Processing*, 33:2404–2418, 2024. 6, 4
- [7] Kevin Clark, Paul Vicol, Kevin Swersky, and David J Fleet. Directly fine-tuning diffusion models on differentiable rewards. In *Proceedings of the International Conference on Learning Representations*, 2025. 2
- [8] Gheorghe Comanici, Eric Bieber, Mike Schaekermann, Ice Pasupat, Noveen Sachdeva, Inderjit Dhillon, Marcel Blistein, Ori Ram, Dan Zhang, Evan Rosen, et al. Gemini 2.5: Pushing the frontier with advanced reasoning, multimodality, long context, and next generation agentic capabilities. *arXiv preprint arXiv:2507.06261*, 2025. 3
- [9] Patrick Esser, Sumith Kulal, Andreas Blattmann, Rahim Entezari, Jonas Müller, Harry Saini, Yam Levi, Dominik Lorenz, Axel Sauer, Frederic Boesel, et al. Scaling rectified flow transformers for high-resolution image synthesis. In *Proceedings of the International Conference on Machine Learning*, 2024. 2
- [10] Ying Fan, Olivia Watkins, Yuqing Du, Hao Liu, Moonkyung Ryu, Craig Boutilier, Pieter Abbeel, Mohammad Ghavamzadeh, Kangwook Lee, and Kimin Lee. Dpokr: Reinforcement learning for fine-tuning text-to-image diffusion models. *Advances in Neural Information Processing Systems*, 36:79858–79885, 2024. 2, 3
- [11] Google. <https://aistudio.google.com/?model=gemini-2.5-flash-image-preview>, 2025. 2, 3, 6
- [12] Daya Guo, Dejian Yang, Haowei Zhang, Junxiao Song, Ruoyu Zhang, Runxin Xu, Qihao Zhu, Shirong Ma, Peiyi Wang, Xiao Bi, et al. Deepseek-r1: Incentivizing reasoning capability in llms via reinforcement learning. *arXiv preprint arXiv:2501.12948*, 2025. 3, 4
- [13] Ziyu Guo, Renrui Zhang, Chengzhuo Tong, Zhizheng Zhao, Peng Gao, Hongsheng Li, and Pheng-Ann Heng. Can we generate images with cot? let’s verify and reinforce image generation step by step. In *Proceedings of the IEEE/CVF Conference on Computer Vision and Pattern Recognition*, 2025. 2
- [14] Pengcheng He, Xiaodong Liu, Jianfeng Gao, and Weizhu Chen. DeBERTaV3: Improving deberta using electra-style pre-training with gradient-disentangled embedding sharing. In *Proceedings of the International Conference on Learning Representations*, 2023. 4
- [15] Edward J Hu, Yelong Shen, Phillip Wallis, Zeyuan Allen-Zhu, Yuanzhi Li, Shean Wang, Lu Wang, Weizhu Chen, et al. Lora: Low-rank adaptation of large language models. *Proceedings of the International Conference on Learning Representations*, 1(2):3, 2022. 6
- [16] Junjie Ke, Qifei Wang, Yilin Wang, Peyman Milanfar, and Feng Yang. Musiq: Multi-scale image quality transformer. In *Proceedings of the IEEE/CVF International Conference on Computer Vision*, pages 5148–5157, 2021. 6, 4
- [17] Yuval Kirstain, Adam Polyak, Uriel Singer, Shahbuland Matiana, Joe Penna, and Omer Levy. Pick-a-pic: An open dataset of user preferences for text-to-image generation. *Advances in neural information processing systems*, 36:36652–36663, 2023. 3
- [18] Black Forest Labs. Flux. <https://github.com/black-forest-labs/flux>, 2023. 2
- [19] Black Forest Labs. Flux.1-kontext-dev. <https://huggingface.co/black-forest-labs/FLUX.1-Kontext-dev>, 2023. 3, 6
- [20] Biwen Lei, Xiefan Guo, Hongyu Yang, Miaomiao Cui, Xuansong Xie, and Di Huang. Abpn: Adaptive blend pyramid network for real-time local retouching of ultra high-resolution photo. In *Proceedings of the IEEE/CVF Conference on Com-*

- puter Vision and Pattern Recognition*, pages 2108–2117, 2022. 2, 3, 6
- [21] Yaron Lipman, Ricky TQ Chen, Heli Ben-Hamu, Maximilian Nickel, and Matt Le. Flow matching for generative modeling. In *Proceedings of the International Conference on Learning Representations*, 2023. 2, 4
- [22] Jie Liu, Gongye Liu, Jiajun Liang, Yangguang Li, Jiaheng Liu, Xintao Wang, Pengfei Wan, Di Zhang, and Wanli Ouyang. Flow-grpo: Training flow matching models via online rl. *Advances in neural information processing systems*, 2025. 2, 3, 4, 6, 1
- [23] Jiaxin Liu, Qichao Ying, Zhenxing Qian, Sheng Li, Runqi Zhang, Jian Liu, and Xinpeng Zhang. MoFRR: Mixture of diffusion models for face retouching restoration. In *Proceedings of the IEEE/CVF International Conference on Computer Vision*, pages 12842–12851, 2025. 3
- [24] Shiyu Liu, Yucheng Han, Peng Xing, Fukun Yin, Rui Wang, Wei Cheng, Jiaqi Liao, Yingming Wang, Honghao Fu, Chunrui Han, et al. Step1x-edit: A practical framework for general image editing. *arXiv preprint arXiv:2504.17761*, 2025. 2, 3
- [25] Xingchao Liu, Chengyue Gong, and Qiang Liu. Flow Straight and Fast: Learning to generate and transfer data with rectified flow. In *Proceedings of the International Conference on Learning Representations*, 2023. 2, 4
- [26] Xin Luo, Jiahao Wang, Chenyuan Wu, Shitao Xiao, Xiyan Jiang, Defu Lian, Jiajun Zhang, Dong Liu, and Zheng Liu. Editscore: Unlocking online rl for image editing via high-fidelity reward modeling. *arXiv preprint arXiv:2509.23909*, 2025. 2, 3, 8
- [27] Chao Ma, Chih-Yuan Yang, Xiaokang Yang, and Ming-Hsuan Yang. Learning a no-reference quality metric for single-image super-resolution. *Computer Vision and Image Understanding*, 158:1–16, 2017. 6, 4
- [28] Vongani H Maluleke, Neerja Thakkar, Tim Brooks, Ethan Weber, Trevor Darrell, Alexei A Efros, Angjoo Kanazawa, and Devin Guillory. Studying bias in gans through the lens of race. In *European Conference on Computer Vision*, pages 344–360. Springer, 2022. 4
- [29] Anish Mittal, Anush K Moorthy, and Alan C Bovik. Making a “completely blind” image quality analyzer. *IEEE Signal Processing Letters*, 20(3):209–212, 2013. 6, 4
- [30] OpenAI. <https://platform.openai.com/docs/models/gpt-image-1>, 2025. 2, 3
- [31] OpenAI, :, Aaron Hurst, Adam Lerer, Adam P. Goucher, Adam Perelman, Aditya Ramesh, and Aidan Clark et al. Gpt-4o system card, 2024. 3
- [32] Mihir Prabhudesai, Anirudh Goyal, Deepak Pathak, and Katerina Fragkiadaki. Aligning text-to-image diffusion models with reward backpropagation. 2023. 2
- [33] Mihir Prabhudesai, Russell Mendonca, Zheyang Qin, Katerina Fragkiadaki, and Deepak Pathak. Video diffusion alignment via reward gradients. *arXiv preprint arXiv:2407.08737*, 2024.
- [34] Rafael Rafailov, Archit Sharma, Eric Mitchell, Christopher D Manning, Stefano Ermon, and Chelsea Finn. Direct preference optimization: Your language model is secretly a reward model. *Advances in neural information processing systems*, 36:53728–53741, 2023. 2, 3
- [35] Team Seedream, Yunpeng Chen, Yu Gao, Lixue Gong, Meng Guo, Qiushan Guo, Zhiyao Guo, Xiaoxia Hou, Weilin Huang, Yixuan Huang, et al. Seedream 4.0: Toward next-generation multimodal image generation. *arXiv preprint arXiv:2509.20427*, 2025. 2, 6
- [36] Alireza Shafaei, James J. Little, and Mark Schmidt. Autoretouch: Automatic professional face retouching. In *Proceedings of the IEEE/CVF Winter Conference on Applications of Computer Vision (WACV)*, pages 990–998, 2021. 3
- [37] Alireza Shafaei, James J Little, and Mark Schmidt. Autoretouch: Automatic professional face retouching. In *Proceedings of the IEEE/CVF Winter Conference on Applications of Computer Vision*, pages 990–998, 2021. 2
- [38] Hossein Talebi and Peyman Milanfar. Nima: Neural image assessment. *IEEE transactions on image processing*, 27(8):3998–4011, 2018. 6, 4
- [39] Sudha Velusamy, Rishubh Parihar, Raviprasad Kini, and Aniket Rege. Fabsoften: Face beautification via dynamic skin smoothing, guided feathering, and texture restoration. In *Proceedings of the IEEE/CVF Conference on Computer Vision and Pattern Recognition Workshops*, pages 530–531, 2020. 3
- [40] Bram Wallace, Meihua Dang, Rafael Rafailov, Linqi Zhou, Aaron Lou, Senthil Purushwalkam, Stefano Ermon, Caiming Xiong, Shafiq Joty, and Nikhil Naik. Diffusion model alignment using direct preference optimization. In *Proceedings of the IEEE/CVF Conference on Computer Vision and Pattern Recognition*, pages 8228–8238, 2024. 2, 3
- [41] Fu-Yun Wang, Yunhao Shui, Jingtian Piao, Keqiang Sun, and Hongsheng Li. Diffusion-npo: Negative preference optimization for better preference aligned generation of diffusion models. In *Proceedings of the International Conference on Learning Representations*, 2025. 2
- [42] Yibin Wang, Zhimin Li, Yuhang Zang, Chunyu Wang, Qinglin Lu, Cheng Jin, and Jiaqi Wang. Unified multimodal chain-of-thought reward model through reinforcement fine-tuning. *Advances in neural information processing systems*, 2025. 4
- [43] Yibin Wang, Yuhang Zang, Hao Li, Cheng Jin, and Jiaqi Wang. Unified reward model for multimodal understanding and generation. *arXiv preprint arXiv:2503.05236*, 2025. 2, 3, 8
- [44] Zhouxia Wang, Jiawei Zhang, Runjian Chen, Wenping Wang, and Ping Luo. Restoreformer: High-quality blind face restoration from undegraded key-value pairs. In *Proceedings of the IEEE/CVF conference on computer vision and pattern recognition*, pages 17512–17521, 2022. 2, 3, 6
- [45] Zhouxia Wang, Jiawei Zhang, Tianshui Chen, Wenping Wang, and Ping Luo. Restoreformer++: Towards real-world blind face restoration from undegraded key-value pairs. *IEEE Transactions on Pattern Analysis and Machine Intelligence*, 45(12):15462–15476, 2023. 3, 6
- [46] Xue Wen, Lianxin Xie, Le Jiang, Tianyi Chen, Si Wu, Cheng Liu, and Hau-San Wong. RetouchFormer: semi-supervised high-quality face retouching transformer with prior-based selective self-attention. In *Proceedings of the AAAI Conference on Artificial Intelligence*, pages 5903–5911, 2024. 2, 3, 6
- [47] Chenfei Wu, Jiahao Li, Jingren Zhou, Junyang Lin, Kaiyuan Gao, Kun Yan, Sheng ming Yin, Shuai Bai, Xiao Xu, Yilei

- Chen, Yuxiang Chen, Zecheng Tang, Zekai Zhang, Zhengyi Wang, An Yang, Bowen Yu, Chen Cheng, Dayiheng Liu, Deqing Li, Hang Zhang, Hao Meng, Hu Wei, Jingyuan Ni, Kai Chen, Kuan Cao, Liang Peng, Lin Qu, Minggang Wu, Peng Wang, Shuting Yu, Tingkun Wen, Wensen Feng, Xiaoxiao Xu, Yi Wang, Yichang Zhang, Yongqiang Zhu, Yujia Wu, Yuxuan Cai, and Zenan Liu. Qwen-image technical report, 2025. 3, 8
- [48] Keming Wu, Sicong Jiang, Max Ku, Ping Nie, Minghao Liu, and Wenhui Chen. Editreward: A human-aligned reward model for instruction-guided image editing. *arXiv preprint arXiv:2509.26346*, 2025. 2, 3, 8
- [49] Xiaoshi Wu, Yiming Hao, Keqiang Sun, Yixiong Chen, Feng Zhu, Rui Zhao, and Hongsheng Li. Human Preference Score v2: A solid benchmark for evaluating human preferences of text-to-image synthesis. *arXiv preprint arXiv:2306.09341*, 2023. 2, 3
- [50] Lianxin Xie, Wen Xue, Zhen Xu, Si Wu, Zhiwen Yu, and Hau San Wong. Blemish-aware and progressive face retouching with limited paired data. In *Proceedings of the IEEE/CVF Conference on Computer Vision and Pattern Recognition*, pages 5599–5608, 2023. 3
- [51] Jiazheng Xu, Xiao Liu, Yuchen Wu, Yuxuan Tong, Qinkai Li, Ming Ding, Jie Tang, and Yuxiao Dong. Imagereward: learning and evaluating human preferences for text-to-image generation. In *Proceedings of the 37th International Conference on Neural Information Processing Systems*, pages 15903–15935, 2023. 2, 3
- [52] Jiazheng Xu, Yu Huang, Jiale Cheng, Yuanming Yang, Jiajun Xu, Yuan Wang, Wenbo Duan, Shen Yang, Qunlin Jin, Shurun Li, et al. Visionreward: Fine-grained multi-dimensional human preference learning for image and video generation. *arXiv preprint arXiv:2412.21059*, 2024. 2
- [53] Zhidan Xu, Xiaoqin Zhang, and Shijian Lu. Face retouching with diffusion data generation and spectral restoration. In *Proceedings of the IEEE/CVF International Conference on Computer Vision*, pages 14722–14731, 2025. 3
- [54] Wen Xue, Le Jiang, Lianxin Xie, Si Wu, Yong Xu, and Hau San Wong. VRetouchEr: Learning cross-frame feature interdependence with imperfection flow for face retouching in videos. In *Proceedings of the IEEE/CVF Conference on Computer Vision and Pattern Recognition*, pages 9141–9150, 2024. 2, 3, 6
- [55] Wen Xue, Chun Ding, Ruotao Xu, Si Wu, Yong Xu, and Hau San Wong. RetouchGPT: LLM-based interactive high-fidelity face retouching via imperfection prompting. In *Proceedings of the AAAI Conference on Artificial Intelligence*, pages 9059–9067, 2025. 2, 3
- [56] Kai Yang, Jian Tao, Jiafei Lyu, Chunjiang Ge, Jiabin Chen, Weihang Shen, Xiaolong Zhu, and Xiu Li. Using human feedback to fine-tune diffusion models without any reward model. In *Proceedings of the IEEE/CVF Conference on Computer Vision and Pattern Recognition*, pages 8941–8951, 2024. 2
- [57] Sidi Yang, Tianhe Wu, Shuwei Shi, Shanshan Lao, Yuan Gong, Mingdeng Cao, Jiahao Wang, and Yujiu Yang. Maniqa: Multi-dimension attention network for no-reference image quality assessment. In *Proceedings of the IEEE/CVF Conference on Computer Vision and Pattern Recognition*, pages 1191–1200, 2022. 6, 4
- [58] Huizhuo Yuan, Zixiang Chen, Kaixuan Ji, and Quanquan Gu. Self-play fine-tuning of diffusion models for text-to-image generation. *Advances in Neural Information Processing Systems*, 37:73366–73398, 2024. 2
- [59] Zechuan Zhang, Ji Xie, Yu Lu, Zongxin Yang, and Yi Yang. In-context edit: Enabling instructional image editing with in-context generation in large scale diffusion transformer. *arXiv preprint arXiv:2504.20690*, 2025. 2, 3, 6
- [60] Huaisheng Zhu, Teng Xiao, and Vasant G Honavar. Dspo: Direct score preference optimization for diffusion model alignment. In *The Thirteenth International Conference on Learning Representations*, 2025. 2

BeautyGRPO: Aesthetic Alignment for Face Retouching via Dynamic Path Guidance and Fine-Grained Preference Modeling

Supplementary Material

A. Mathematical Derivations for Dynamic Path Guidance

A.1. From Flow-Matching ODE to SDE (Flow-GRPO)

Flow-Matching ODE. In flow-matching generative models, a deterministic ordinary differential equation (ODE) is used to transport a simple noise distribution $p_1(x)$ at time $t = 1$ to the data distribution $p_0(x)$ at $t = 0$ along a continuous trajectory. The model learns a time-dependent vector field $v_\theta(x, t)$ such that integrating

$$dx_t = v_\theta(x_t, t) dt \quad (11)$$

evolves x_t from pure noise at $t = 1$ to a realistic sample x_0 at $t = 0$. Strictly following this learned ODE trajectory typically yields high-fidelity images. However, a deterministic path is incompatible with exploration in a reinforcement learning (RL) setting: we need stochasticity to explore alternative outcomes and obtain diverse reward signals.

ODE-to-SDE conversion (FlowGRPO). FlowGRPO [22] converts the deterministic ODE into a stochastic differential equation (SDE) while preserving the marginal distributions of the original ODE at every time t . Specifically, it injects Gaussian noise at each sampling step in exploration process:

$$dx_t = \left[v_\theta(x_t, t) + \frac{\sigma_t^2}{2t} (x_t + (1-t)v_\theta(x_t, t)) \right] dt + \sigma_t d\omega_t, \quad (12)$$

where $d\omega_t$ denotes the increment of a standard Wiener process, which can be approximated as $d\omega_t \approx \sqrt{dt} \epsilon_t$, with $\{\epsilon_t\}$ i.i.d. $\mathcal{N}(0, I)$ across time steps, and $\sigma_t = \eta \sqrt{\frac{t}{1-t}}$ controls the noise magnitude at time t .

Here the SDE in Eq. (12) is formulated in reverse time (from $t = 1$ to $t = 0$). For a small timestep Δt , the Euler-Maruyama discretization of Eq. (12) yields the conditional mean

$$\mu_t = x_t + \left[v_\theta(x_t, t) + \frac{\sigma_t^2}{2t} (x_t + (1-t)v_\theta(x_t, t)) \right] \Delta t, \quad (13)$$

with a step-wise standard deviation

$$\sigma_{\text{step}} = \sigma_t \sqrt{\Delta t}. \quad (14)$$

The one-step update can therefore be written as

$$x_{t-\Delta t} = \mu_t + \sigma_{\text{step}} z_t, \quad z_t \sim \mathcal{N}(0, I), \quad (15)$$

where z_t is a standard normal random vector. Eqs. (13)–(15) show that each update is centered at the model prediction μ_t and then perturbed by isotropic Gaussian noise, so iterating this stochastic update produces a distribution over possible final states x_0 rather than a single deterministic outcome, which in turn enables the policy to explore multiple image variants under the same condition and obtain diverse reward feedback in the RL setting.

A.2. Fidelity–Exploration Conflict

While the SDE in FlowGRPO provides the stochasticity needed for online RL, it conflicts with the high-fidelity requirements of face retouching. From the discrete update in Eq. 15, each noise sample z_t perturbs the state away from the model-predicted mean μ_t , and the cumulative term

$$\sum_t \sigma_{\text{step}}(t) z_t$$

over T sampling steps (we discretize the exploration process into T steps) gradually drives the trajectory $\{x_t\}$ off the high-quality image manifold. Here $\sigma_{\text{step}}(t) = \sigma_t \sqrt{\Delta t}$ denotes the step-wise standard deviation at time t . In generic text-to-image generation this drift can be tolerable or even helpful for diversity, but in face retouching it mainly appears as noise artifacts. Reducing σ_t mitigates drift but also suppresses exploration, limiting the ability of RL to find higher-reward solutions. We therefore introduce a mechanism that keeps the trajectory close to a high-fidelity manifold while still enabling controlled stochastic exploration.

A.3. Dynamic Path Guidance (DPG)

To resolve the fidelity–exploration conflict, we introduce Dynamic Path Guidance (DPG), which performs anchored exploration by reshaping the noise in the FlowGRPO SDE so that the sampling trajectory remains close to a high-fidelity reference path while still preserving stochasticity.

Anchor-guided target. We assume access to a high-quality anchor sample x_0^{anchor} that lies on the desired high-fidelity manifold (e.g., a top-rated retouched face from our preference dataset). At sampling time t with current state x_t , we construct a straight-line path connecting x_t to x_0^{anchor} over the remaining sampling-time horizon. The corresponding target at the next time $t - \Delta t$ on this anchor-guided path is defined as

$$x_{t-\Delta t}^* = \left(1 - \frac{\Delta t}{t}\right) x_t + \frac{\Delta t}{t} x_0^{\text{anchor}}, \quad (16)$$

which is a linear interpolation that moves a fraction $\Delta t/t$ of the distance from x_t toward x_0^{anchor} . Geometrically, $x_{t-\Delta t}^*$ lies on the segment joining x_t and x_0^{anchor} and specifies an anchor-consistent reference direction for the next update. In practice, t is discretized into T sampling timesteps in the exploration process and we only apply the anchor-guided update for $t > 0$, so the division by t is well-defined and the final step at $t = 0$ is treated as the terminal state.

Anchor correction noise. Recall that the FlowGRPO discretization in Eq. (15) can be written as

$$x_{t-\Delta t} = \mu_t + \sigma_{\text{step}} z_t, \quad z_t \sim \mathcal{N}(0, I), \quad (17)$$

where μ_t is given by Eq. (13) and $\sigma_{\text{step}} = \sigma_t \sqrt{\Delta t}$. Conditioned on x_t , this induces the Gaussian transition

$$x_{t-\Delta t} | x_t \sim \mathcal{N}(\mu_t, \sigma_{\text{step}}^2 I). \quad (18)$$

The noise that maps the next state exactly to the anchor-guided target $x_{t-\Delta t}^*$ in Eq. (16) is obtained by enforcing

$$x_{t-\Delta t}^* = \mu_t + \sigma_{\text{step}} z_t, \quad (19)$$

which yields the anchor correction vector

$$z_t^{\text{anchor}} = \frac{x_{t-\Delta t}^* - \mu_t}{\sigma_{\text{step}}}. \quad (20)$$

The vector z_t^{anchor} in Eq. (20) precisely maps the next state onto the anchor-guided target $x_{t-\Delta t}^*$. However, if this correction is applied deterministically at every step, i.e., $z_t = z_t^{\text{anchor}}$ for all t , then $x_{t-\Delta t} = x_{t-\Delta t}^*$ holds throughout the sampling process, causing the trajectory to collapse onto the deterministic anchor path in Eq. (16) and leaving no space for stochastic exploration.

Mixed noise and time-dependent guidance. To retain stochasticity, DPG replaces the original standard Gaussian z_t with a time-dependent mixture of the anchor correction and an independent standard normal sample. Let $z_t^{\text{std}} \sim \mathcal{N}(0, I)$ be independent of x_t and define

$$z_t^{\text{mix}} = \lambda_t z_t^{\text{anchor}} + (1 - \lambda_t) z_t^{\text{std}}, \quad 0 \leq \lambda_t \leq 1, \quad (21)$$

where λ_t is a time-dependent guidance weight. In practice, we discretize the reverse-time sampling process into T steps indexed by integers $t \in \{0, \dots, T-1\}$, where T denotes the total number of steps in the exploration process. We adopt the same linear schedule as in the main text,

$$\lambda_t = \frac{t}{\max(1, T-1)}. \quad (22)$$

Sampling proceeds in reverse time from $t = T-1$ (early, high-noise steps) down to $t = 0$ (late refinement), so the effective guidance weight λ_t is large at early sampling timesteps and gradually decreases to 0 toward the final refinement steps. For notational simplicity, we continue to write

λ_t in the derivations below to denote this time-dependent weight. We then replace z_t in the discretization above by z_t^{mix} and obtain the DPG transition

$$x_{t-\Delta t} = \mu_t + \sigma_{\text{step}} z_t^{\text{mix}}. \quad (23)$$

Conditioned on x_t , the anchor correction z_t^{anchor} is a deterministic function of $(x_t, x_0^{\text{anchor}})$ and the only stochastic component is z_t^{std} . Taking conditional expectation with respect to z_t^{std} and using $\mathbb{E}[z_t^{\text{std}}] = 0$, we obtain

$$\mathbb{E}[x_{t-\Delta t} | x_t] = \mu_t + \sigma_{\text{step}} \mathbb{E}[z_t^{\text{mix}} | x_t] \quad (24)$$

$$= \mu_t + \sigma_{\text{step}} \lambda_t z_t^{\text{anchor}} \quad (25)$$

$$= \mu_t + \lambda_t (x_{t-\Delta t}^* - \mu_t) \quad (26)$$

$$= (1 - \lambda_t) \mu_t + \lambda_t x_{t-\Delta t}^*. \quad (27)$$

Thus, in expectation, DPG interpolates the transition mean between the original FlowGRPO mean μ_t and the anchor-guided target $x_{t-\Delta t}^*$, with interpolation weight λ_t .

Similarly, still conditioning on x_t and treating z_t^{anchor} as deterministic, the covariance of z_t^{mix} is

$$\text{Cov}[z_t^{\text{mix}} | x_t] = (1 - \lambda_t)^2 I, \quad (28)$$

since z_t^{anchor} has zero conditional variance and $\text{Cov}[z_t^{\text{std}}] = I$. This implies

$$x_{t-\Delta t} | x_t \sim \mathcal{N}\left((1 - \lambda_t) \mu_t + \lambda_t x_{t-\Delta t}^*, ((1 - \lambda_t) \sigma_{\text{step}})^2 I\right). \quad (29)$$

When $\lambda_t = 0$, Eq. (29) reduces exactly to the original FlowGRPO kernel with mean μ_t and variance $\sigma_{\text{step}}^2 I$. When $\lambda_t = 1$, the variance collapses to zero and the update becomes a deterministic step to $x_{t-\Delta t}^*$. For intermediate values $0 < \lambda_t < 1$, the trajectory is biased toward the anchor path while retaining a reduced but nonzero variance.

Effect on fidelity and exploration. Eqs. (27) and (29) show that DPG simultaneously (i) pulls the mean transition toward an anchor-consistent direction and (ii) shrinks the step variance by a factor of $(1 - \lambda_t)^2$. By choosing λ_t large when t is large and the state is still highly noisy, the sampling trajectory in the exploration process is tightly constrained around the high-fidelity anchor manifold during the early, structure-forming stages. As $t \rightarrow 0$ and $\lambda_t \rightarrow 0$, the variance gradually recovers to its original level, allowing finer stochastic exploration on top of an already well-structured face. In this way, DPG reconciles the fidelity requirements of portrait retouching with the exploration needs of online reinforcement learning, purely through a sampling-time modification of the FlowGRPO transition kernel without changing the underlying flow-matching policy v_θ .

B. Anchored Exploration with Standard GRPO Optimization

It is important to emphasize that the anchor image is employed exclusively during the sampling-based exploration

phase that generates trajectories for GRPO, and it is never used as a supervision target in the optimization objective. During the exploration phase, for each input portrait in FRPref-10K, we select a high-quality retouched image as the anchor x_0^{anchor} solely to construct the DPG-guided sampling path. Specifically, at each sampling timestep t , DPG computes the anchor-guided target $x_{t-\Delta t}^*$ and the corresponding correction noise z_t^{anchor} (Eqs. (16)–(20)), forms the mixed noise z_t^{mix} in Eq. (21), and updates $x_{t-\Delta t}$ via Eq. (23). This anchored exploration only changes how trajectories $\{x_t\}$ are sampled during RL rollouts and does not add any reconstruction or regression term toward the anchor in the loss.

In the optimization phase, we apply the standard GRPO objective to the policy model π_θ . The reward model scores the final retouched outputs x_0 , and these scores are converted into advantages to optimize the policy via the clipped GRPO loss. This optimization process is entirely independent of the anchor image. In particular, the anchor image x_0^{anchor} is never used as a pixel-level or feature-level target, and there is no supervised alignment between the policy output and the anchor. At inference time, DPG is discarded entirely, and we utilize standard ODE sampling. This ensures that the inference process requires no reference images and incurs no additional computational cost.

C. Relation to Reference-Guided Methods, CFG, and Path Regularization

Although DPG uses an anchor image during the exploration phase, its role and implementation are fundamentally different from typical reference-guided editing, classifier-free guidance (CFG), or path regularization.

Distinction from Reference-Guided Editing. Conventional reference-based methods explicitly inject the reference image into the model architecture as an additional conditioning signal (e.g., via concatenation, cross-attention, or style codes), often training the network to strictly imitate the reference appearance through supervised losses. In contrast, our anchor image is never passed through the retouching network as an input condition and never appears in the optimization objective. Instead, it serves purely as a geometric anchor to define an anchor-based ODE path in the latent space and to compute the correction noise z_t^{anchor} within the sampler. The policy model π_θ remains conditioned solely on the original input portrait and textual prompt, learning aesthetic alignment from reward signals rather than through direct supervision against the anchor.

Distinction from Classifier-Free Guidance (CFG). CFG modifies the sampling dynamics by adding a guidance term proportional to the difference between conditional and unconditional model outputs. This effectively steers the generation toward regions with higher likelihood under the condition. In contrast, DPG operates without an external classifier or dual-forward passes. Instead of altering the

Table 5. Distortion vs. perceptual quality metrics on FFHQ.

Method	PSNR \uparrow	SSIM \uparrow	LPIPS \downarrow	MUSIQ \uparrow	MANIQA \uparrow	NRQM \uparrow	
SUPERVISED	RetouchFormer	42.088	0.997	0.024	4.465	1.036	8.175
	Xu (2025) [53]	45.480	0.993	0.008	–	–	–
	RetouchGPT	46.210	–	0.002	–	–	–
GENERATIVE	ICEdit	32.463	0.882	0.152	4.192	0.978	7.424
	SeedDream	25.598	0.739	0.170	4.503	0.993	7.538
	NanoBanana	28.841	0.824	0.106	4.681	1.009	8.065
	Flux.K w/LoRA	36.001	0.956	0.063	4.459	1.035	8.009
	Ours	33.697	0.927	0.102	4.906	1.079	8.401

vector field, DPG reshapes the stochastic transition kernel by linearly mixing a deterministic anchor correction with standard Gaussian noise via a time-dependent weight λ_t . This simultaneously biases the transition mean toward the anchor-guided direction (Eq. (27)) and shrinks the variance (Eq. (29)), keeping the trajectory on a high-fidelity manifold during early sampling while still allowing exploration. All of this is achieved without requiring auxiliary guidance networks or modifying the drift prediction.

Distinction from Path Regularization. Path regularization methods typically enforce that the learned vector field or sampling trajectory stay close to a predefined reference path by adding explicit regularization terms to the training loss, penalizing deviations over the entire trajectory. Our DPG does not add any path penalty or consistency term to the loss function. The anchor-based ODE path is used only at sampling time to construct $x_{t-\Delta t}^*$ and z_t^{anchor} , and the influence of the anchor is further modulated by the schedule λ_t that decays along the sampling timesteps. Thus, DPG acts as a sampling-time constraint on exploration rather than a training-time path regularizer. It regularizes the rollout distribution from which GRPO collects experience, while the GRPO objective itself remains unchanged.

Summary. DPG distinguishes itself from these methods in that: (i) the anchor image is neither a supervised target nor an explicit conditioning input; (ii) no auxiliary guidance network or classifier is employed; and (iii) no regularization terms are added to the training loss. Instead, DPG is a lightweight exploration-time mechanism that reshapes the SDE sampling kernel using anchor-induced geometry, enabling high-fidelity yet exploratory RL updates while keeping inference-time sampling identical to standard ODE-based flow matching.

D. Evaluation Metrics

D.1. Why Not Use Full-Reference Metrics

Previous face retouching works [20, 44, 46, 54] typically adopt classical full-reference (FR) metrics, such as PSNR, SSIM, and LPIPS, to assess pixel-level fidelity between the retouched output and a ground-truth reference. However, we maintain that FR metrics are fundamentally ill-suited for

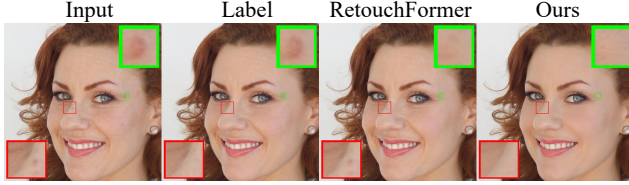


Figure 8. Visual examples of imperfect ground-truth references in the FFHQ dataset, which are actively corrected by our method.

evaluating aesthetic enhancement tasks like face retouching, supported by both theoretical and empirical evidence:

- **Theoretical Conflict (The Perception-Distortion Trade-off).** As theoretically justified by Blau and Michaeli [5], there is an inherent mathematical conflict between maximizing perceptual quality and minimizing pixel-level distortion (e.g., PSNR). Specifically, models strictly minimizing distortion tend to average out high-frequency details, often resulting in overly smoothed and perceptually flat skin textures. In contrast, synthesizing realistic facial details, such as natural pores and lighting variations, inevitably introduces pixel-wise deviations from the reference. This tradeoff is clearly evident in Table 5: compared to our supervised baseline (Flux.K w/LoRA), our RL-optimized BeautyGRPO trades pixel fidelity (PSNR dropping from 36.00 to 33.70 dB) for significant aesthetic gains (MUSIQ improving from 4.46 to 4.91). Optimizing strictly for FR metrics fundamentally restricts a model’s ability to achieve peak perceptual quality.
- **Imperfect Ground Truth and Defect Replication.** FR metrics implicitly assume that target reference images are flawless. In reality, existing datasets like FFHQ often contain ground-truth references with residual blemishes or suboptimal aesthetic qualities (see Fig. 8). Models optimizing for high PSNR are therefore forced to replicate these defects to strictly match the reference. In contrast, BeautyGRPO actively corrects these flaws, moving beyond the dataset’s inherent limitations to improve naturalness and visual appeal. Consequently, FR metrics unfairly penalize our model for deviating from these flawed references.

Consequently, we focus on no-reference (NR) metrics, which directly evaluate naturalness, realism, and aesthetic quality, providing a much more accurate and reliable reflection of true human preference in face retouching.

D.2. No-Reference Metrics

For these reasons, we instead focus on no-reference (NR) perceptual and aesthetic metrics that better approximate human judgments in our evaluation.

- **NIQE [29] (↓).** NIQE models the statistical regularities of high-quality natural images and measures how strongly a test image deviates from them. For face retouching, it mainly reflects global perceptual naturalness, including



Figure 9. Age and racial distribution of the FRPref-10K dataset.

whether skin texture appears artificial, overly smooth, or oily, and whether it contains visible AI artifacts. A **lower** score indicates better perceptual naturalness.

- **NIMA [38] (↑).** NIMA predicts the distribution of human opinion scores and uses the expected rating as the aesthetic quality measure. The AVA-trained model emphasizes overall visual appeal, including composition, color harmony, and aesthetic preference. A **higher** score indicates better aesthetic quality.
- **MUSIQ [16] (↑).** MUSIQ provides a holistic assessment of perceptual quality by jointly considering texture fidelity, clarity, and overall aesthetic impression. The AVA-trained model is sensitive to global balance as well as fine-grained visual quality, making it suitable for evaluating portrait enhancements. A **higher** score indicates better perceptual quality.
- **NRQM [27] (↑).** NRQM predicts a single perceptual quality score learned from subjective studies. In face retouching, it reflects perceived sharpness, texture realism, and local structure fidelity, especially in facial regions. A **higher** score indicates better perceptual quality.
- **MANIQA [57] (↑).** MANIQA is designed to detect complex distortions and generative artifacts. It is particularly sensitive to texture integrity, fine facial detail, and subtle artifacts introduced during retouching. A **higher** score indicates better perceptual and textural quality.
- **TOPIQ [6] (↑).** TOPIQ follows a top-down procedure that emphasizes distortions in semantically important regions. Using the GFIQA-trained face model, it focuses on face-region clarity, texture naturalness, and identity preservation. A **higher** score indicates better face-specific perceptual quality.

E. Composition and Statistics of FRPref-10K

To ensure a diverse and representative training corpus for aesthetic alignment, we carefully curated the FRPref-10K dataset. The dataset comprises a mixture of sources: 70% of the images are sampled from the official training split of the FFHQ dataset, while the remaining 30% are sourced from a proprietary high-resolution portrait collection. This hybrid approach specifically helps mitigate racial and demographic biases [28] present in FFHQ datasets. To provide a comprehensive understanding of the dataset’s diversity, we detail its demographic distribution in Fig. 9.

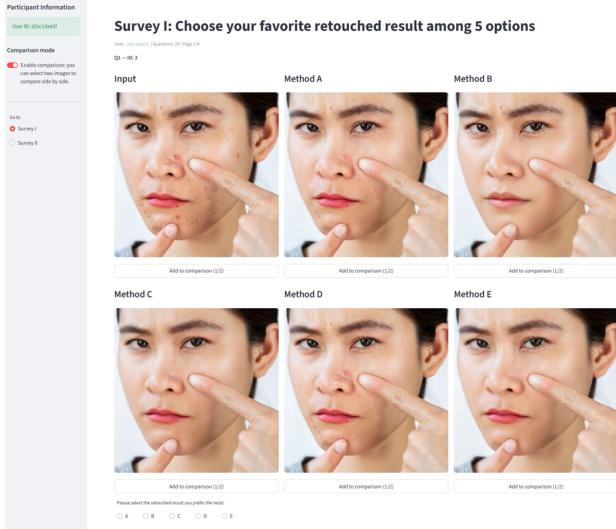


Figure 10. User interface of Questionnaire I.

F. User Study Details

F.1. Study Protocol

We design two complementary questionnaires to evaluate users’ perceptual preferences and to assess how well different reward models align with human judgments.

Questionnaire I: Overall Preference. The first questionnaire consists of a fixed set of 25 questions. Each question presents one original input portrait and five retouched results produced by different methods, including our approach and representative baselines. For each question, participants are asked to select one retouched image that they personally prefer the most. We do not impose any additional instructions or constraints, and users are encouraged to follow their first impression and choose according to their own subjective aesthetic preferences. The 25 questions cover a diverse range of ages, genders, and ethnicities, and the candidate images in each question include both clearly different cases and more subtle differences in texture and details. To reduce position bias, the order of the five candidate images within each question is randomized. The user interface of Questionnaire I is illustrated in Figure 10.

Questionnaire II: Dimension-wise Ratings for Reward Evaluation. The second questionnaire is designed to measure the consistency between different reward models and human judgments on fine-grained perceptual dimensions. It is constructed from an additional pool of 20 input–output pairs. For each participant, 5 questions are randomly sampled from this pool. Each question shows one original portrait and one retouched result, and users rate the result along five dimensions: skin smoothing, blemish removal, skin texture quality, clarity, and identity preservation. For each dimen-

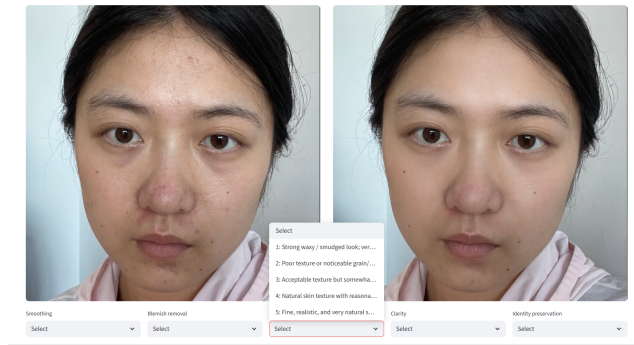


Figure 11. User interface of Questionnaire II.

sion, participants assign an integer score in the range 0–5, where a larger value indicates better perceived quality. We provide a detailed textual description and concrete examples for every score level of each dimension (from 0 to 5), so that users have a clear and consistent guideline when rating. These human scores are later compared with the outputs of different reward models to quantify their alignment with human perception. The user interface of Questionnaire II is illustrated in Figure 11.

Data Collection and Aggregation. In total, we obtain 100 valid questionnaires from anonymous participants. For Questionnaire I, we compute the win rate of each method as the proportion of answers in which it is selected as the preferred result over all questions and participants. For Questionnaire II, we aggregate the human scores for each dimension by averaging over all participants and questions, and then compare these averages with the corresponding scores predicted by different reward models. This allows us to evaluate dimension-wise consistency between reward models and human judgments.

F.2. Demographic Analysis of User Preferences

Figure 12 presents the win rates for Questionnaire I, stratified by user age group and gender. Our method achieves the highest win rate in every demographic group, consistently capturing at least 50% of user preferences and reaching about 75% for women aged 18–24 and 45+ years. Competing methods obtain much smaller shares, with none exceeding 25% in any group or showing consistent dominance for any demographic. These results indicate that the preference advantage of our method is robust across ages and genders, rather than being driven by a single specific subgroup.

G. Training Details

G.1. Reward Model Training Details

We adopt Qwen2.5-VL-7B-Instruct [2] as our base reward model. For both SFT stages (Stage 1 and Stage 2), training

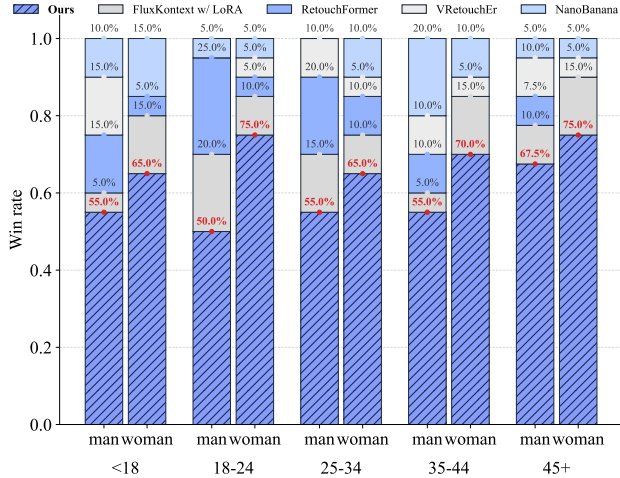


Figure 12. Comparison of user preference win rates for various face retouching methods across different ages and gender.

is performed with a per-device batch size of 1, 8 gradient accumulation steps, a learning rate of 5×10^{-5} , and a warm-up ratio of 0.1. For the GRPO stage, we use a per-device batch size of 2, 4 gradient accumulation steps, a learning rate of 1×10^{-6} , and a warm-up ratio of 0.05, with a KL penalty coefficient $\beta = 0.04$. The number of generated responses N is set to 8.

G.2. Retouching Model Training Configuration

We adopt Flux.1 Kontext [19] as our base retouching model and first perform LoRA adaptation on our face retouching corpus. The model is trained at a resolution of 1024×1024 with LoRA rank 32 and $\alpha = 32$, using AdamW with a learning rate of 1×10^{-5} , cosine learning rate decay, 500 warm-up steps, weight decay 0.01, a per-device batch size of 4, and 2 gradient accumulation steps. For BeautyGRPO, we initialize from this LoRA-adapted Flux.1 Kontext and run online RL at 1024×1024 resolution with a per-device batch size of 2 and 8 images per prompt, using $T = 10$ sampling steps and a noise level $\eta = 0.7$.

H. CoT Reasoning Examples of Reward Model

We provide qualitative examples of our reward model’s Chain-of-Thought (CoT) reasoning process in Figure 13.

I. More Visual Results

Figures 14–16 provide additional qualitative comparisons across different face retouching methods, further highlighting the perceptual advantages of our BeautyGRPO.

J. Discussion and Future Work

J.1. Anchor Selection and Quality

In our main experiments, we use the top-1 high-preference sample as the anchor x_0^{anchor} for each input, which keeps the implementation simple and ensures that the anchor lies on a high-fidelity manifold. Conceptually, DPG only requires the anchor to be a reasonably good exemplar that constrains exploration to a high-quality neighborhood while still allowing the policy to move beyond it when the reward signal suggests a better solution. Systematic studies of alternative anchor selection strategies (e.g., sampling from a top- k set, diversity-aware anchors, or combining multiple anchors) are promising directions for future work.

J.2. Scenarios Without Explicit Anchors

In this work, we focus on a practical face-retouching regime where each input portrait is accompanied by at least one high-quality retouched exemplar (e.g., curated or highly rated images in FRPref-10K), which naturally provides anchors for DPG. In scenarios where only raw inputs are available and no such exemplars exist, one could instead construct pseudo-anchors using a strong reward model, self-distilled EMA policies, or other generative priors, and then apply the same anchored-exploration principle. Exploring such anchor-free or weakly anchored settings is an interesting extension of DPG that we leave to future work.

J.3. DPG at Inference Time

We apply DPG only during the sampling-based exploration phase of RL training. After optimization, standard ODE sampling uses the improved vector field to produce high-fidelity results without anchors or extra computation at inference time. In principle, one could design inference-time variants of DPG by supplying reference images or synthesizing anchors on the fly, but this would introduce additional assumptions and complexity. We therefore adopt pure ODE sampling for deployment and leave inference-time extensions of DPG as future work.



Input



Image1



Image2





<think>

You are a professional portrait beauty enhancement evaluation expert with expertise in semantic image understanding, facial structure analysis, and aesthetic judgment.
 Your task is: Based on the user-provided three images: one original image (Input) and two beautified result images (Image1 and Image2), systematically analyze the editing operations applied to the two beautified images relative to the Input. For each dimension, evaluate both the editing intensity and the editing quality.

You must zoom in on local regions to examine pixel-level details, and pay special attention to the following five dimensions:

1. Skin smoothing effect: Whether the Input's facial skin has been moderately smoothed, reasonably reducing pores and fine lines in the forehead, cheeks, nose wings, corners of the mouth, and eye area, while keeping it within a natural range and avoiding plastic-like texture or complete loss of pores.
2. Blemish removal effect: Whether facial blemishes in the Input, such as spots, acne, pimples, or uneven skin tone, have been effectively removed.
3. Skin tone and texture effect: Evaluate the skin tone, facial glow, and texture to determine whether the skin looks more aesthetically pleasing.
4. Preservation of personal features: Whether important personal features are fully preserved (e.g., male facial hair, female makeup, elderly wrinkles, moles, and freckles), without deletion or weakening.
5. Overall clarity: Refers to the global image quality, i.e., whether the contours of facial features (eyes, lips, nose bridge) are sharp and clear, and whether there is any blurriness, noise, or AI artifacts.

For each dimension, compare Image1 and Image2 relative to the Input, and assign an integer score from 1 to 5 (higher scores indicate better results). Strictly use the following output structure:

1. All reasoning and analysis must be written inside:
<think> ... </think>
2. All scoring and the final judgment must be written inside:
<answer>...</answer>

[Scoring Section]

1. Skin smoothing effect: Image1 = X, Image2 = Y
2. Blemish removal effect: Image1 = X, Image2 = Y
3. Skin tone and texture effect: Image1 = X, Image2 = Y
4. Preservation of personal features: Image1 = X, Image2 = Y
5. Overall clarity: Image1 = X, Image2 = Y

Image1 = X.XX, Image2 = Y.YY

[Preference Judgment]

ImageX is better

</answer>

<think>

1. Skin smoothing effect:
 - Image1 applies a light to moderate smoothing effect. Fine lines on the forehead and around the eyes are slightly reduced, but skin texture is still visible, maintaining a natural look.
 - Image2 applies a much stronger smoothing effect. The forehead lines are nearly erased, and the cheeks and under-eye areas appear overly airbrushed, resulting in a plastic-like texture and loss of natural skin detail.
2. Blemish removal effect:
 - Image1 removes minor blemishes and evens out the skin tone slightly, but some unevenness remains, especially around the cheeks and jawline.
 - Image2 removes all visible blemishes and discoloration, achieving a very clean and uniform skin appearance.
3. Skin tone and texture effect:
 - Image1 retains a natural skin tone with slight enhancement in brightness and warmth, giving a healthy and realistic appearance.
 - Image2 has a flatter, more artificial tone. The skin appears waxy and lacks natural glow or texture, making it look less lifelike.
4. Preservation of personal features:
 - Image1 preserves all personal features such as facial structure, hair texture, and natural lines.
 - Image2 slightly alters the facial structure, especially around the eyes and cheeks, due to over-smoothing. Some natural contours are lost.
5. Overall clarity:
 - Image1 maintains sharpness in the eyes, lips, and hair. The image is crisp and detailed.
 - Image2 shows slight blurring in the facial features, especially around the eyes and mouth, likely due to aggressive smoothing.

</think>

<answer>

[Scoring Section]

1. Skin smoothing effect: Image1 = 4, Image2 = 2 \n2. Blemish removal effect: Image1 = 4, Image2 = 5 \n3. Skin tone and texture effect: Image1 = 5, Image2 = 1 \n4. Preservation of personal features: Image1 = 5, Image2 = 3 \n5. Overall clarity: Image1 = 5, Image2 = 3

[Average Score] Image1 = 4.6, Image2 = 2.8

[Preference Judgment] Image1 is better.

</answer>

Figure 13. Qualitative examples of face retouching CoT reward reasoning. Given an input image and two retouched candidates, our reward model performs chain-of-thought quality assessment across five dimensions: skin smoothing, blemish removal, skin texture quality, clarity, and identity preservation.



Figure 14. Visual comparison of face retouching results across different methods on the FFHQR dataset, where Flux.K denotes FluxKontext. Compared with existing methods that suffer from incomplete blemish removal, over-smoothing, or unnatural visual appearance, our BeautyGRPO cleanly removes blemishes while preserving identity-consistent natural skin texture, gloss, and fine details such as wrinkles.

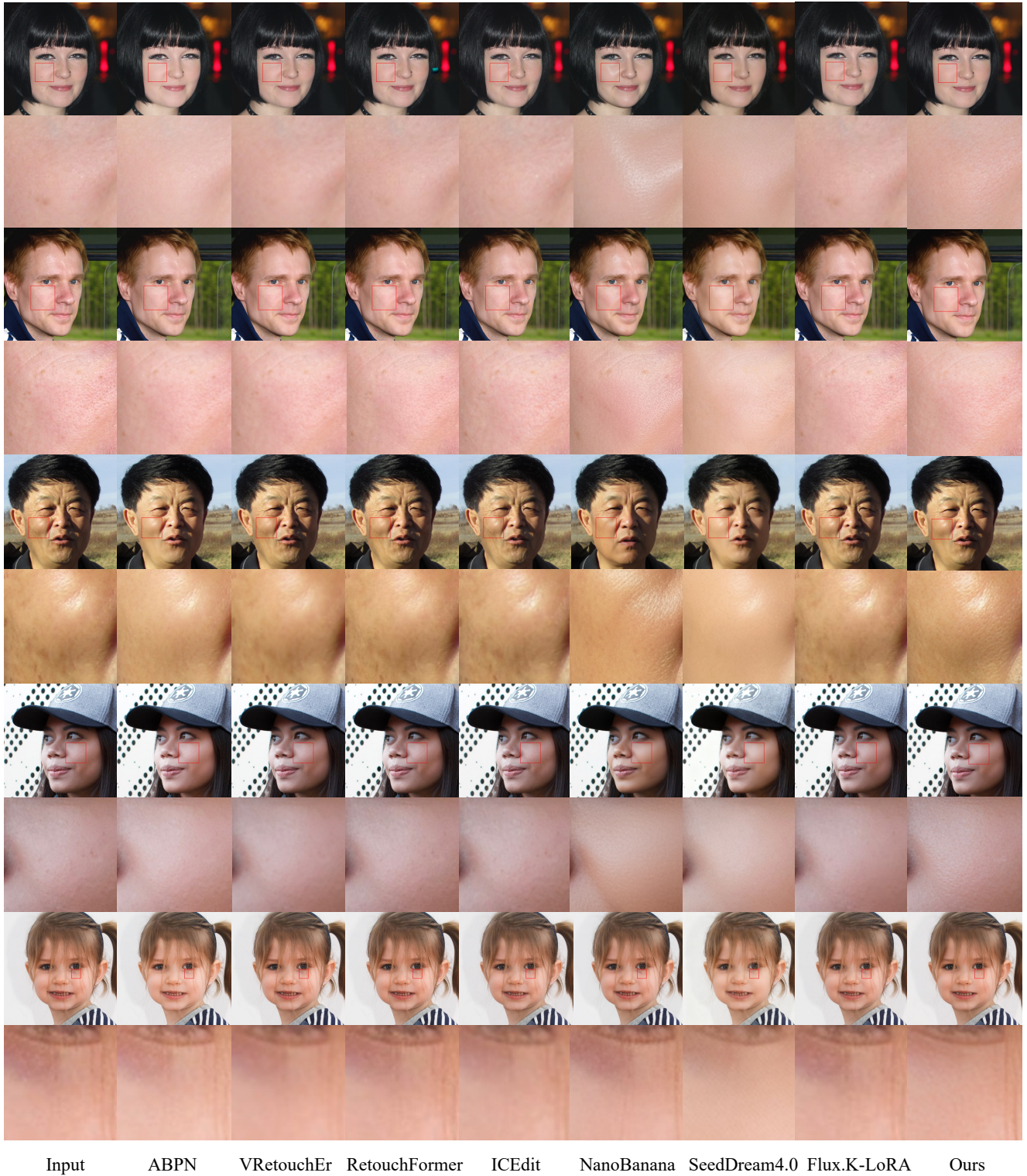


Figure 15. Visual comparison of face retouching results across different methods on the FFHQR dataset, where Flux.K denotes FluxKontext. Compared with existing methods that suffer from incomplete blemish removal, over-smoothing, or unnatural visual appearance, our BeautyGRPO cleanly removes blemishes while preserving identity-consistent natural skin texture, gloss, and fine details such as wrinkles.



Figure 16. Visual comparison of face retouching results across different methods on in-the-wild datasets, where Flux.K denotes FluxKontext. Compared with existing methods that suffer from incomplete blemish removal, over-smoothing, or unnatural visual appearance, our BeautyGRPO cleanly removes blemishes while preserving identity-consistent natural skin texture, gloss, and fine details such as moles.